IEEE Access
Multidisciplinary | Rapid Review | Open Access Journal

Received October 22, 2021, accepted November 16, 2021, date of publication November 25, 2021,
date of current version December 13, 2021.

Digital Object Identifier 10.1109/ACCESS.2021.3130601

Analysis of FD-NOMA Cognitive Relay System With Interference From Primary User Under Maximum Average Interference Power Constraint

HOANG VAN TOAN[1], QUYET-NGUYEN VAN[2], TRAN MANH HOANG[3], VAN-DUC PHAN[4], BUI VU MINH[5], PHAM THANH HIEP[6], (Member, IEEE), AND LE THE DUNG[7,8], (Member, IEEE)

[1]Faculty of Telecommunications, Telecommunications University, Nha Trang, Khanh Hoa 650000, Vietnam
[2]Faculty of Technology, Dong Nai University of Technology, Bien Hoa 76163, Vietnam
[3]Faculty of Radio, Telecommunications University, Nha Trang, Khanh Hoa 650000, Vietnam
[4]Faculty of Automobile Technology, Van Lang University, Ho Chi Minh City 700000, Vietnam
[5]Faculty of Automotive, Mechanical, Electrical and Electronic Engineering, Nguyen Tat Thanh University, Ho Chi Minh City 700000, Vietnam
[6]Faculty of Radio Electronics, Le Quy Don Technical University, Hanoi 100000, Vietnam
[7]Division of Computational Physics, Institute for Computational Science, Ton Duc Thang University, Ho Chi Minh City 70000, Vietnam
[8]Faculty of Electrical and Electronics Engineering, Ton Duc Thang University, Ho Chi Minh City 70000, Vietnam

Corresponding author: Le The Dung (lethedung@tdtu.edu.vn)

ABSTRACT In this paper, we consider a non-orthogonal multiple access (NOMA) based underlay cognitive radio (CR) system consisting of a source, two destinations, and a relay in the secondary network. The source communicates with two destinations using the NOMA technique via the assistance of the relay operating in full-duplex (FD) mode. The operations of all secondary nodes are affected by the interference from a primary transmitter. Meanwhile, secondary transmitters must adjust their transmission powers so that the interference probability to a primary receiver is always less than a given value. Under this average interference power constraint, we propose the maximum average interference power (MAIP) constraint for the relay to achieve its highest possible average transmit power. Based on the MAIP constraint, we derive the exact closed-form expression of the outage probabilities and ergodic capacities at two destination users. Monte-Carlo simulations verify the accuracy of the obtained mathematical expressions. Numerical results show that the considered NOMA-FD-CR relay system's performance is significantly affected by the interference from the primary transmitter and the maximum tolerable interference of the primary receiver. Additionally, using the MAIP constraint at the relay substantially improves the quality of the received signal at the far user with a slight reduction in the signal quality at the near user and fulfills the interference constraint without needing the instantaneous channel state information (CSI).

INDEX TERMS NOMA, full-duplex, cognitive radio, outage probability, ergodic capacity.

I. INTRODUCTION

Cognitive radio (CR) technology stems from the problem of radio frequency spectrum scarcity in the context of increasing demand for the number and the access speed of wireless services [1], [2]. In the CR technology, secondary users (not licensed to use spectrum) can share radio frequency spectrum with primary users (licensed to use spectrum) as long as the secondary user's operation does not affect the primary user. There are three main types of CR techniques: underlay CR, overlay CR, and interweave CR. Among those, the underlay CR is the most popular because of its feasibility in the fifth-generation (5G) radio system. The principle of underlay CR is that the secondary transmitters (STs) must continuously adjust their transmission power so that the total interferences from STs to the primary receiver (PR) are always less than a predetermined threshold. On the other hand, the rapid development of mobile communication systems and the Internet of Things (IoT) offers new requirements and challenges for the 5G wireless systems [3]. Compared with 4G wireless systems, the quality-of-service (QoS) that the 5G wireless systems have to achieve are very high. For example, the spectrum efficiency increases 5 to 15 times; the number of connections can be dozen times higher with at least

The associate editor coordinating the review of this manuscript and approving it for publication was Prakasam Periasamy.

10^6 connections/km^2; small delay (less than 1ms), and efficient support for different radio services [4].

Regarding multiple access techniques, the frequency division multiple access (FDMA), time division multiple access (TDMA), code division multiple access (CDMA), and orthogonal frequency division multiple access (OFDMA) are the common ones used in wireless systems [5], [6]. In these orthogonal multiple access (OMA) techniques, radio resources are orthogonally divided over time, frequency, code for multiple users or based on the combination of these parameters. However, the OMA technique has some major disadvantages, e.g., the number of users is limited, ensuring the signal orthogonality is difficult. Therefore, to meet the demand for an increasing number of connections in the 5G wireless systems, the non-orthogonal multiple access (NOMA) technique has been proposed. The main idea of the NOMA technique is to support the non-orthogonal identification of radio resources among users. It can be classified into two main categories: power-domain NOMA [7] and code-domain NOMA [8]. Many works in the literature have combined NOMA with other novel technologies to create new systems that meet higher performance requirements. For instance, the authors in [9], [10] combined NOMA and full-duplex (FD) to achieve high spectral efficiency because the FD relay help to improve the spectral efficiency of wireless systems because the signal can be received and transmitted simultaneously [11]. Besides, NOMA has also been applied in various emerging topics of wireless communications such as energy harvesting [12], [13], physical layer security [14], short-packet communications [15].

II. RELATED WORKS

Lv *et al.* [16] proposed the cooperative transmission scheme to exploit the spatial diversity of an underlay CR-NOMA system, where a base station (BS) provided unicast and multicast services to a primary user (PU) and a group of secondary users (SUs). The closed-form analytical results showed that the cooperative transmission scheme gave better system performance when more SUs participated in relaying and ensured the full diversity order at SU and a diversity order of two at PU. In [17], a NOMA-assisted cooperative overlay spectrum sharing framework for multi-user CR networks was developed. Specifically, a SU was scheduled to help forward the primary signal and its signal by applying the NOMA technique and two other proposed schemes. The results revealed that these two schemes could achieve a full diversity order for the primary and secondary transmissions. Lee *et al.* [18] investigated a cooperative NOMA scheme in an underlay CR network by deriving the approximate closed-form expression of the outage probability (OP) of the SU for single-user and multi-user scenarios. It was shown that the cell-edge user with poor channel gain could benefit from both cooperative NOMA and opportunistic relay transmission. Chu and Zepernick [19] proposed a power-domain NOMA scheme for cooperative CR networks. In particular, a decode-and-forward (DF) secondary relay was deployed to decode the superimposed signals of two SUs. Then, a power-domain NOMA was employed to forward the signals from this relay to two SUs based on the channel power gains of the corresponding two links. Mathematical expressions for the OP and ergodic capacity of each secondary user were derived. Arzykulov *et al.* [20] examined an underlay CR-NOMA network with amplify-and-forward (AF) relaying. The closed-form OP expressions of SU were derived, and the OP results for CR-NOMA were compared with those for CR-OMA. Bariah *et al.* [21] analyzed the error rate performance of relay-assisted NOMA with partial relay selection in an underlay CR network. The authors derived an accurate closed-form pairwise error probability (PEP) expression for the power-constrained SUs with successive interference cancellation (SIC), then used it to evaluate the bit error rate (BER) and solved an optimization problem to find the optimal power allocation coefficients that minimize the BER union bound under average power and individual union bound constraints. Im and Lee [22] studied a cooperative NOMA system with imperfect SIC in an underlay CR network. Considering that the channel coefficients between the primary transmitter (PT) and secondary receivers (SRs follow the Rayleigh distribution, the authors derived the exact closed-form and asymptotic OP expressions for two cases, i.e., when the interference constraint goes to infinity and when the transmission power of secondary source and relay goes to infinity.

All previous works assumed that the relays operated in half-duplex (HD). However, FD and NOMA techniques have been applied to relays in CR networks to improve spectral efficiency further. Notably, Aswathi and Babu [23] considered an underlay CR-NOMA system, where the near user acted as a full/half-duplex DF relay for the far user. The authors derived the closed-form OP expressions and determined the optimal power allocation coefficient at the secondary transmitter that minimizes the system OP. Mohammadali *et al.* [24] proposed a joint optimization problem of relay beamforming and the transmit powers at the BS and cognitive relay to maximize the rate of the near user in an FD relay assisted NOMA-CR network. The results demonstrated that FD relaying with the proposed optimum and suboptimal schemes significantly enhanced the data rates of both near and far users compared to the HD relaying. This work was then extended into [25] by including the exact closed-form expressions for the outage probability of three fixed zero forcing-based precoding schemes. Unfortunately, the interference effect from PT to SR was not considered. In underlay CR systems, we should note that the transmission power of the ST is limited because it is not allowed to affect the operation of the primary system. As a result, the coverage of the ST is also small, which means that the SR locates not too far from the PR. Therefore, assuming that the interference from PT to SR is negligible as in [25] is not realistic. On the other hand, one of the most significant difficulties when analyzing FD relay systems' performance is to consider the simultaneous interference effect of all STs on the PRs. Moreover, adjusting the transmission power of the ST so

that the total interfering power at the PR does not exceed a predetermined threshold is a problem that has not been completely resolved. Specifically, it was only considered as a constraint in optimization problems without giving any specific mathematical expressions for the transmission power of ST. On the other hand, combining FD and NOMA techniques is an efficient way to improve the spectral efficiency of next-generation wireless systems. Thus, the FD-CR-NOMA systems have attracted increasing attention in the literature, such as [26]–[28]. Especially, the works in [26], [27] considered the secondary and primary users as two NOMA users; thus, allocating power for these two users is challenging. Singh and Upadhyay [28] analyzed an overlay cognitive system. However, it is widely known that the overlay CR systems do not support real-time communications for secondary users. Additionally, the link between source and near secondary user was not considered.

In short, all previous works only mentioned the interference constrain from secondary network to primary network but lacked the impact of interference caused by the primary network to the second network. On the other hand, combining FD and NOMA techniques in a system is an efficient way to improve the spectral efficiency of next-generation wireless systems. Motivated by the above observations, in this paper, we analyze a NOMA-FD-CR system model, taking into account the interference effect from the PT to the SRs. The contributions of this paper can be summarized as follows:

- We analyze the performance of a NOMA-CR system where an FD relay assists the communication between a source and two destinations in the secondary network. To overcome the limitations of previous works in the literature and for practical purposes, we consider the interference from the PT to the SRs. It is a crucial problem to be investigated in future cognitive radio systems.
- We propose the maximum average interference power (MAIP) constraint for the relay to achieve the highest possible transmission power at the relay while ensuring that the total interference power at the PRs does not exceed a predetermined maximum tolerable interference level. Applying the MAIP constraint at the relay helps to improve the quality of the received signal at the far user significantly while only reduce the performance of the signal at the near user slightly.
- We give an explicit expression of the relay's transmission power such that the interference probability of the STs to the PR is always less than a predefined threshold. Based on this transmission power constraint, we derive the exact closed-form expressions of the outage probabilities and ergodic capacities at two destination users.
- We conduct Monte-Carlo simulations to verify the correctness of the derived mathematical expressions. All analysis results closely match the simulation ones. It is demonstrated that the performance of the considered FD-NOMA-CR relay system depends much on the interference from the PT and the maximum tolerable inference of the PR. Furthermore, the interference constraint can be fulfilled if the ST's average transmission power is appropriately adjusted. More importantly, the considered FD-CR-NOMA system provides lower OP and higher EC than the HD-CR-NOMA system.

The rest of the paper is organized as follows. Section III describes the considered system and channel models. Section IV focuses on deriving the exact closed-form expressions of the outage probabilities and ergodic capacities of two secondary destinations. Numerical results and the corresponding discussions are presented in Section V. Finally, some conclusions are given in Section VI.

For the sake of clarity, we provide in Table 1 the notations along with their descriptions used in this paper.

TABLE 1. The mathematical notations used in this paper.

Notation	Description
$Pr(\cdot)$	Probability of an event
$F_X(x)$	Cumulative distribution function (CDF)
$f_X(x)$	Probability density function (PDF)
$\mathcal{CN}(\mu, \sigma^2)$	Complex Gaussian distribution with mean μ and variance σ^2
λ_{XY}	Average channel gain between X and Y terminals
$\tilde{P}_{\mathrm{S}}, \tilde{P}_{\mathrm{R}}, \tilde{P}_{\mathrm{T}}$	Transmission power of source, relay, and primary transmitter
$\tilde{I}_{\mathrm{P}}$	Interference threshold of primary receiver
$\tilde{I}_{\mathrm{R}}$	Residual self-interference of full-duplex relay
$\tilde{P}_{\mathrm{R}}^{\mathrm{AIP}}$	Average interference power constraint
$\tilde{P}_{\mathrm{R}}^{\mathrm{MAIP}}$	Maximum interference power constraint
$E_i(z)$	Exponential integral function
$\mathcal{W}(\cdot)$	Lambert function
a_1, a_2	Power allocation coefficients for signals x_{A} and x_{B}

III. SYSTEM MODEL

The secondary network consists of a source (S) transmitting signals to two destinations A and B by using the NOMA technique. Since B is far from S, it needs an assistance in data forwarding from a DF full-duplex relay R. The primary network includes a PT and a PR as shown in Fig. 1. It is assumed that all nodes are equipped with a single antenna. The channel coefficients offer that the flat Rayleigh fading, i.e., the magnitude fixed in each time slot and vary in next blocks. The channel gain between X and Y, is denote as $|h_{\mathrm{XY}}|^2$, and assuming as exponential distributed with the probability density function (PDF) and the cumulative distribution function (CDF) are, respectively, given by

$$f_{|h_{\mathrm{XY}}|^2}(z) = \frac{1}{\lambda_{\mathrm{XY}}} e^{-\frac{z}{\lambda_{\mathrm{XY}}}}, \tag{1}$$

$$F_{|h_{\mathrm{XY}}|^2}(z) = 1 - e^{-\frac{z}{\lambda_{\mathrm{XY}}}}. \tag{2}$$

A. TRANSMISSION POWER CONSTRAINTS

In CR systems, the interference from STs to the PRs must not exceed an allowed threshold $\tilde{I}_{\mathrm{P}}$. The interference constraints can be classified into three types [29]: (i) *average interference constraint*: ST has to adjust the average power so that the interference probability (interference power greater than $\tilde{I}_{\mathrm{P}}$) at the input of PR is lower than a predefined threshold ϕ [30];

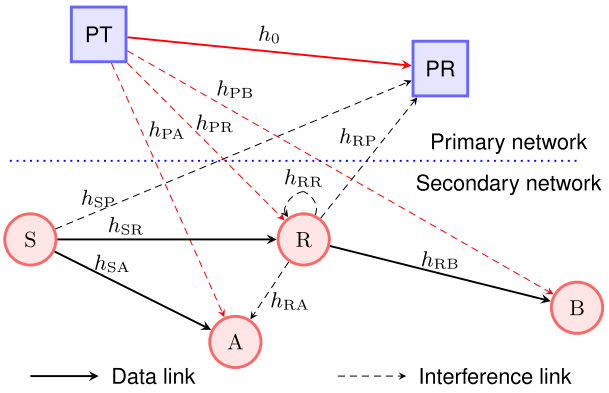

FIGURE 1. System model of downlink cognitive NOMA relay system with FD relay.

(ii) *simultaneous interference constraint*: the STs have to adjust the simultaneous transmission powers so that the interference power at PR does not exceed $\tilde{I}_P$ [31]; (iii) *interference constraint based on the SINR at PR*: ST has to adjust the transmission power so that the SINR at PR is always larger than a predefined threshold or the QoS of primary network is always ensured [32]. The interference constraint based on the SINR at PR requires that ST knows the CSI from PT to PR. However, this requirement is not realistic because the operations of PUs and SU are independent. In the simultaneous interference constraint, ST always updates PR on its CSI quickly and accurately to not interfere with the PR. This requirement sets high criteria for the channel estimation from ST to PR at the PR. The CSI is then sent back to ST quickly and accurately, or reversible channel property can be used in specific circumstances. In summary, the average interference constraint is easy to implement in practice and allows a more straightforward system architecture.

In our considered NOMA-FD-CR relay system, since two nodes S and R simultaneously transmit signals, they cause interferences to the PR. Consequently, the power allocation and adjustment for these STs are difficult. On the other hand, the average constraint condition from the ST to the PR is imposed on the system. Particularly, depending on the QoS of primary network, the PR accepts an interference probability threshold ϕ, with $0 < \phi < 1$. The interference constraint from ST to PR is presented as

$$\Pr\left(\tilde{P}_S|h_{SP}|^2 + \tilde{P}_R|h_{RP}|^2 \geq \tilde{I}_P\right) \leq \phi, \tag{3}$$

where $\tilde{P}_S$ and $\tilde{P}_R$ are the transmission power of S and R, respectively.

Assuming that the interference caused by S to the PR satisfies the condition

$$\Pr\left(\tilde{P}_S|h_{SP}|^2 \geq \alpha\tilde{I}_P\right) \leq \phi, \tag{4}$$

where α, $0 \leq \alpha \leq 1$, is the interference distribution factor.

Then, the transmission power of S must satisfy the following condition

$$\Pr\left(\tilde{P}_S|h_{SP}|^2 \geq \alpha\tilde{I}_P\right) \leq \phi$$
$$\Leftrightarrow e^{-\frac{\alpha\tilde{I}_P}{\tilde{P}_S\lambda_{SP}}} \leq \phi \Leftrightarrow \tilde{P}_S \leq \frac{\alpha\tilde{I}_P}{\lambda_{SP}\ln\left(\frac{1}{\phi}\right)}. \tag{5}$$

Therefore, the best transmission power of S is selected as

$$\tilde{P}_S = \frac{\alpha\tilde{I}_P}{\lambda_{SP}\ln\left(\frac{1}{\phi}\right)}. \tag{6}$$

Given this transmission power of S, we need to find the transmission power of R so that the interferences simultaneously caused by S and R to the PR fulfill the constraint in (3). Usually, to satisfy the constraint in (3), previous studies as [25], [33] used the interference distribution factor α to divide the maximum tolerable interfering power corresponding to the transmitters in the secondary system. Consequently, the transmission power of R is adjusted to satisfy

$$\Pr\left(\tilde{P}_R|h_{RP}|^2 \geq (1-\alpha)\tilde{I}_P\right) \leq \phi. \tag{7}$$

In this scenario, namely the average interference power (AIP) constraint, the average transmission power of R that satisfies the constraints in (7) can be determined as

$$\tilde{P}_R^{AIP} = \frac{(1-\alpha)\tilde{I}_P}{\lambda_{RP}\ln\left(\frac{1}{\phi}\right)}. \tag{8}$$

In the considered system, we can see that the transmission power of R greatly affects the quality of the received signal at B. Therefore, the transmission power of R must be as high as possible as long as the interference constraint in (3) is satisfied. However, if we consider the interference of R or S separately as the function of α in the case of AIP constraint, the average transmission power of R given in (8) cannot reach the maximum value.

Instead, the best transmission power of R is the value that satisfies

$$\Pr\left(\tilde{P}_S|h_{SP}|^2 + \tilde{P}_R|h_{RP}|^2 \geq \tilde{I}_P\right) = \phi. \tag{9}$$

Applying the result in Appendix A, we obtain

$$\frac{\tilde{P}_S\lambda_{SP}}{\tilde{P}_S\lambda_{SP} - \tilde{P}_R\lambda_{RP}} e^{\frac{-\tilde{I}_P}{\tilde{P}_S\lambda_{SP}}} - \frac{\tilde{P}_R\lambda_{RP}}{\tilde{P}_S\lambda_{SP} - \tilde{P}_R\lambda_{RP}} e^{\frac{-\tilde{I}_P}{\tilde{P}_R\lambda_{RP}}} = \phi. \tag{10}$$

From the result of Appendix A, we can choose the best transmission power of R in this scenario, namely maximum average interference power (MAIP) constraint, $\tilde{P}_R^{MAIP}$, as

$$\tilde{P}_R^{MAIP} = \frac{\omega_3\tilde{I}_P}{\omega_3\lambda_{RP}\mathcal{W}\left(\frac{\tilde{I}_P}{\omega_3}\exp\left(\frac{\tilde{I}_P\phi}{\omega_3}\right)\right) - \phi\tilde{I}_P\lambda_{RP}} \tag{11}$$

where $\omega_3 = \tilde{P}_S\lambda_{SP}\left(e^{-\frac{\tilde{I}_P}{\tilde{P}_S\lambda_{SP}}} - \phi\right)$ and $\mathcal{W}(\cdot)$ denotes the Lambert function [34].

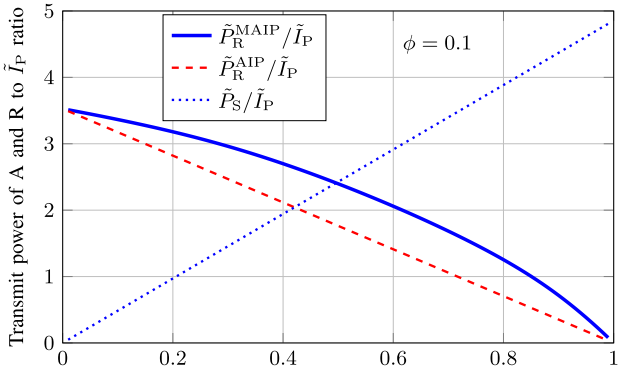

FIGURE 2. Ratio of $\tilde{P}_R^{MAIP}$, $\tilde{P}_R^{AIP}$, and $\tilde{P}_S$ to $\tilde{I}_P$ versus the interference distribution coefficient α for $\phi = 0.1$.

For the comparison between the transmission power of R in the case of AIP constraint and that in the case of MAIP constraint, we plot in Fig. 2 the ratios of $\tilde{P}_S$, $\tilde{P}_R^{AIP}$, and $\tilde{P}_R^{MAIP}$ to $\tilde{I}_P$ versus α for different interference probability threshold ϕ. We can see that linearly increasing the transmission power of S decreases the transmission power of R. However, $\tilde{P}_R^{MAIP}/\tilde{I}_P$ decreases in the form of a parabolic curve. In contrast, $\tilde{P}_R^{AIP}/\tilde{I}_P$ linearly decreases in the form of a straight line. Moreover, $\tilde{P}_R^{MAIP}$ is always greater than $\tilde{P}_R^{AIP}$. Therefore, using the transmission power as (11) for MAIP constraint will improve the performance of user B. It is also noted that the main goal of the considered system is using the relay R to improve the signal quality at far user B. Thus, we will employ the MAIP constraint in the considered system. For the sake of simplicity in mathematical equations, the transmission power of R corresponding to MAIP constraint, $\tilde{P}_R^{MAIP}$, is denoted as $\tilde{P}_R$ hereafter.

B. SIGNAL MODEL

According to the coding principle of NOMA technique, S transmits to both A and B a combination of the intended signal, i.e.,

$$x_S[n] = \sqrt{\tilde{P}_S a_1} x_A[n] + \sqrt{\tilde{P}_S a_2} x_B[n], \quad (12)$$

where x_A and x_B denotes the signals intended for A and B, respectively; a_1 and a_2 represent the power allocation coefficients for A and B such that $a_1 + a_2 = 1$ and $a_1 < a_2$.

Then, the received signal at A is

$$y_A[n] = h_{SA} x_S[n] + \sqrt{\tilde{P}_T} h_{PA} x_{PU}[n] + \sqrt{\tilde{P}_R} h_{RA} x_B[n-\tau] + n_A[n], \quad (13)$$

where $n_A[n] \sim \mathcal{CN}\left(0, \sigma_{A,n}^2\right)$ is the additive white Gaussian noise (AWGN) at A; τ, $\tau \geq 1$, refers to the time delay caused by FD relay processing at R [35].

Remark 1: In this system, we implicitly assume that the relay operates in the HD mode in the first τ time slots because there is no symbol to transmit. Hence, x_B and x_A are decoded at A by using the SIC technique without being interfered by R. From the next $(\tau + 1)$ time slot, R operates in the FD mode. Then, A is affected by the interference from R due to $x_B[\tau + 1]$ transmitting signals. Fortunately, A can now recognize the $x_B[\tau + 1]$ signal because it already decoded x_B in the first τ time slots; thus, A applies the SI cancellation technique to suppress the interference effectively.

Based on the decoding principle of the NOMA technique, A first decodes x_B by treating x_A as interference. Hence, the SINR for decoding x_B at A in the first step is

$$\gamma_{x_A \to x_B} = \frac{\tilde{P}_S a_2 |h_{SA}|^2}{\tilde{P}_S a_1 |h_{SA}|^2 + \tilde{P}_R |h_{RA}|^2 + \tilde{P}_T |h_{PA}|^2 + \sigma_{A,n}^2}. \quad (14)$$

As stated in Remark 1, A can utilize SI cancellation technique to cancel $x_B[n-\tau]$ transmitted by R. However, it is difficult to cancel $x_B[n-\tau]$ completely, therefore, the channel from R to A can be modeled as an inter-user interference channel whose channels coefficient is determined as $h_{RA} \sim CN(0, k\lambda_{RA})$ [25], where k indicates the strength of inter-user interference.

After decoding x_B successfully in the first step, A cancels x_B and decodes the desired x_A in the second step. The SINR for decoding x_A at A can be expressed as

$$\gamma_{x_A} = \frac{\tilde{P}_S a_1 |h_{SA}|^2}{\tilde{P}_R |h_{RA}|^2 + \tilde{P}_T |h_{PA}|^2 + \sigma_{A,n}^2}. \quad (15)$$

The received signal at R can be written as

$$y_R[n] = h_{BR} x_S[n] + \sqrt{\tilde{P}_T} h_{PR} x_{PU}[n] + \sqrt{\tilde{P}_R} h_{RR} x_B[n-\tau] + n_R[n], \quad (16)$$

where $n_R[n] \sim \mathcal{CN}\left(0, \sigma_{R,n}^2\right)$ is the AWGN at R.

Since x_B is assigned with a larger power allocation coefficient, R will first decode x_B by treating x_A as interference. On the other hand, R can recognize $x_B[n-\tau]$; thus, it uses SI cancellation technique to eliminate $x_B[n-\tau]$ in the loop interference when operating in FD mode. However, R cannot eliminate $x_B[n-\tau]$ completely. As a result, there exists a residual self-interference (RSI). Moreover, it is noted that the loop interference after the propagation domain cancellation exhibits the Rayleigh distribution because the SI cancellation in the analog and digital domain involves reconstruction of the SI signal to remove it from the received signal. Thus, the RSI is the error induced by the imperfect reconstruction (mainly due to imperfect loop interference channel estimation) [36]. In addition, since the digital-domain cancellation is carried out after a quantization operation, it is clear that the RSI after three-domain SI cancellation no longer follows the Rayleigh distribution but is more reasonable to be modeled as a normal (Gaussian) random variable. Therefore, the RSI is presented as a complex Gaussian random variable with mean zero, and variance $\tilde{I}_R$ [37], [38]. Then, the SINR for decoding x_B at R is given by

$$\gamma_{x_B}^R = \frac{\tilde{P}_S a_2 |h_{SR}|^2}{\tilde{P}_S a_1 |h_{SR}|^2 + \tilde{P}_T |h_{PR}|^2 + \tilde{I}_R + \sigma_{R,n}^2}. \quad (17)$$

At user B, the received signal can be expressed as

$$y_{\mathrm{B}}[n]=\sqrt{\tilde{P}_{\mathrm{R}}}h_{\mathrm{RB}}x_{\mathrm{B}}[n-\tau]+\sqrt{\tilde{P}_{\mathrm{T}}}h_{\mathrm{PB}}x_{\mathrm{PU}}[n]+n_{\mathrm{B}}[n] \quad (18)$$

where $n_{\mathrm{B}}[n] \sim \mathcal{CN}\left(0, \sigma^2_{\mathrm{B,n}}\right)$ is the AWGN at B.

Therefore, the SINR at B is given by

$$\gamma^{\mathrm{B}}_{x_{\mathrm{B}}} = \frac{\tilde{P}_{\mathrm{R}}|h_{\mathrm{RB}}|^2}{\tilde{P}_{\mathrm{T}}|h_{\mathrm{PB}}|^2+\sigma^2_{\mathrm{B,n}}}. \quad (19)$$

From the above signal model, the interference caused by primary network to secondary network, i.e., $\sqrt{\tilde{P}_{\mathrm{T}}}h_{\mathrm{PA}}$, $\sqrt{\tilde{P}_{\mathrm{T}}}h_{\mathrm{PR}}$, and $\sqrt{\tilde{P}_{\mathrm{T}}}h_{\mathrm{PB}}$, are studied for the first time in this paper.

IV. PERFORMANCE ANALYSIS

In this section, we focus on mathematically analyzing two important system metrics, i.e., the outage probability and ergodic capacity of two users.

A. OUTAGE PROBABILITY (OP)

1) THE OP OF THE NEAR USER A, $P_{\mathrm{out,A}}$

The OP of user, $P_{\mathrm{out,A}}$, is determined as the probability that A cannot decode x_{B} in the first step or can decode signal x_{B} in the first step but fails to decode x_{A} in the second step. Mathematically, $P_{\mathrm{out,A}}$ is calculated as

$$P_{\mathrm{out,A}} = 1-\Pr\left(\gamma^{\mathrm{A}}_{x_{\mathrm{B}}\to x_{\mathrm{A}}} > \gamma_2, \gamma^{\mathrm{A}}_{x_{\mathrm{A}}} > \gamma_1\right), \quad (20)$$

where $\gamma_1 = 2^{R_{\mathrm{A}}}-1$, $\gamma_2 = 2^{R_{\mathrm{B}}}-1$, R_{A} and R_{B} are the target rates of x_{A} and x_{B} at A and B, respectively.

Sine $\mathcal{X}$ and $\mathcal{Y}$ are exponential random variables, i.e., $\mathcal{X} \sim \mathcal{CN}(0,\lambda_x)$, $\mathcal{Y} \sim \mathcal{CN}(0,\lambda_y)$; $\mathcal{Z} = a\mathcal{X}+b\mathcal{Y}$, where a and b are two positive real numbers. The PDF of $\mathcal{Z}$, $f_{\mathcal{Z}}(z)$, is determined as [7]

$$f_{\mathcal{Z}}(z) = \frac{1}{a\lambda_x - b\lambda_y}\left(e^{-\frac{z}{a\lambda_x}} - e^{-\frac{z}{b\lambda_y}}\right). \quad (21)$$

For the convenience of mathematical analysis, we assume $\sigma^2_{\mathrm{A,n}} = \sigma^2_{\mathrm{R,n}} = \sigma^2_{\mathrm{B,n}} = \sigma^2$. Moreover, we set $X = |h_{\mathrm{BA}}|^2$, $W = P_{\mathrm{R}}|h_{\mathrm{RA}}|^2 + P_{\mathrm{T}}|h_{\mathrm{PA}}|^2$, $P_{\mathrm{T}} = \tilde{P}_{\mathrm{T}}/\sigma^2$, $P_{\mathrm{S}} = \tilde{P}_{\mathrm{S}}/\sigma^2$, $P_{\mathrm{R}} = \tilde{P}_{\mathrm{R}}/\sigma^2$, $\mathrm{I}_{\mathrm{R}} = \tilde{\mathrm{I}}_{\mathrm{R}}/\sigma^2$. Then, $P_{out,x_{\mathrm{A}}}$ can be rewritten as

$$P_{out,\mathrm{A}} = 1-\Pr\left(\frac{P_{\mathrm{S}}a_2X}{P_{\mathrm{S}}a_1X+W+1} > \gamma_2, \frac{P_{\mathrm{S}}a_1X}{W+1} > \gamma_1\right). \quad (22)$$

After some mathematical manipulations, $P_{out,x_{\mathrm{A}}}$ is determined in the following Theorem 1.

Theorem 1: The exact closed-form expression of the OP of the near user in the considered NOMA-FD-CR relay system is given by

$$P_{out,\mathrm{A}} = \begin{cases} 1 - e^{-\frac{\theta}{P_{\mathrm{S}}\lambda_{\mathrm{SA}}}}\left(\frac{1}{P_{\mathrm{R}}k\lambda_{\mathrm{RA}}-P_{\mathrm{T}}\lambda_{\mathrm{PA}}}\right) \\ \times\left(\frac{P_{\mathrm{R}}P_{\mathrm{S}}k\lambda_{\mathrm{RA}}\lambda_{\mathrm{SA}}}{P_{\mathrm{R}}\theta k\lambda_{\mathrm{RA}}+P_{\mathrm{S}}\lambda_{\mathrm{SA}}} - \frac{P_{\mathrm{T}}P_{\mathrm{S}}\lambda_{\mathrm{PA}}\lambda_{\mathrm{SA}}}{P_{\mathrm{T}}\theta\lambda_{\mathrm{PA}}+P_{\mathrm{S}}\lambda_{\mathrm{SA}}}\right) \\ \quad \text{if } a_2-a_1\gamma_2>0, \\ 1 \quad \text{if } a_2-a_1\gamma_2<0, \end{cases} \quad (23)$$

where $\theta = \max\left(\frac{\gamma_2}{(a_2-a_1\gamma_2)}, \frac{\gamma_1}{a_1}\right)$.

Proof: See Appendix B.

2) THE OP OF THE FAR USER B, $P_{\mathrm{out,B}}$

Since the received signal at B is forwarded by the FD relay R, the OP at B, $P_{\mathrm{out,B}}$, is determined as the probability that R cannot decode x_{B} or R decode successfully x_{B} but node B cannot decode successfully x_{B}. Mathematically, $P_{\mathrm{out,B}}$ can be computed as

$$\begin{aligned} P_{out,\mathrm{B}} &= 1-\Pr\left(\gamma^{\mathrm{R}}_{x_{\mathrm{B}}} > \gamma_2, \gamma^{\mathrm{B}}_{x_{\mathrm{B}}} > \gamma_2\right) \\ &= 1-\Pr\left(\gamma^{\mathrm{R}}_{x_{\mathrm{B}}} > \gamma_2\right)\Pr\left(\gamma^{\mathrm{B}}_{x_{\mathrm{B}}} > \gamma_2\right). \end{aligned} \quad (24)$$

Theorem 2: The exact closed-form expression of the far user B in the considered NOMA-FD-CR relay system is given by

$$P_{out,\mathrm{B}} = \begin{cases} 1 - e^{-\left(\frac{\gamma_2(\mathrm{I}_{\mathrm{R}}+1)}{P_{\mathrm{S}}(a_2-a_1\gamma_2)\lambda_{\mathrm{SR}}}+\frac{\gamma_2}{P_{\mathrm{R}}\lambda_{\mathrm{RB}}}\right)} \\ \times\frac{P_{\mathrm{S}}(a_2-a_1\gamma_2)\lambda_{\mathrm{SR}}}{P_{\mathrm{S}}(a_2-a_1\gamma_2)\lambda_{\mathrm{SR}}+P_{\mathrm{T}}\gamma_2\lambda_{\mathrm{PR}}} \\ \times\frac{P_{\mathrm{R}}\lambda_{\mathrm{RB}}}{\gamma_2P_{\mathrm{T}}\lambda_{\mathrm{PB}}+P_{\mathrm{R}}\lambda_{\mathrm{RB}}} \quad \text{if } a_2-a_1\gamma_2>0, \\ 1 \quad \text{if } a_2-a_1\gamma_2<0. \end{cases} \quad (25)$$

Proof: See Appendix C.

From (23) and (25), we can see that the power allocation coefficients a_1 and a_2 must satisfy $a_1 < \frac{a_2}{2^{R_{\mathrm{B}}}-1}$ to ensure the fair performance of A and B. On the other hand, the RSI I_R only impacts $P_{\mathrm{out,B}}$ but not $P_{\mathrm{out,A}}$, while the interference from PT affects both $P_{\mathrm{out,A}}$ and $P_{\mathrm{out,B}}$. In addition, the target rates R_{A} and R_{B} also influence $P_{\mathrm{out,A}}$ and $P_{\mathrm{out,B}}$, smaller R_{A} and R_{B} results in smaller $P_{\mathrm{out,A}}$ and $P_{\mathrm{out,B}}$.

B. ERGODIC CAPACITY (EC)

1) THE EC OF x_{A}

The EC of x_{A} over S−A channel is calculated as

$$C_{x_{\mathrm{A}}} = \int_0^\infty \log_2(1+x) f_{\gamma_{x_{\mathrm{A}}}}(x)\,dx. \quad (26)$$

Using integration by parts, we can express (26) in terms of the CDF of $\gamma_{x_{\mathrm{A}}}$, i.e.,

$$C_{x_{\mathrm{A}}} = \frac{1}{\ln 2}\int_0^\infty \frac{1-F_{\gamma_{x_{\mathrm{A}}}}(x)}{1+x}dx. \quad (27)$$

The EC of x_{A} at A is determined in the following Theorem 3.

Theorem 3: The exact analytical expression of the EC of x_{A} at A in the considered NOMA-FD-CR relay system with the interference from PT is given by

$$\begin{aligned} C_{x_{\mathrm{A}}} &= \frac{1}{(c_1-1)\ln 2}\left(\frac{P_{\mathrm{S}}a_1\lambda_{\mathrm{SA}}}{P_{\mathrm{R}}k\lambda_{\mathrm{RA}}-P_{\mathrm{T}}\lambda_{\mathrm{PA}}}\right) \\ &\times\left(e^{\frac{-c_1}{P_{\mathrm{S}}a_1\lambda_{\mathrm{SA}}}}\mathrm{E}i\left(\frac{-c_1}{P_{\mathrm{S}}a_1\lambda_{\mathrm{SA}}}\right) - e^{-\frac{1}{P_{\mathrm{S}}a_1\lambda_{\mathrm{SA}}}}\mathrm{E}i\left(\frac{1}{P_{\mathrm{S}}a_1\lambda_{\mathrm{SA}}}\right)\right) \end{aligned}$$

$$-\frac{1}{(d_1-1)\ln 2}\left(\frac{P_S a_1\lambda_{SA}}{P_R k\lambda_{RA}-P_T\lambda_{PA}}\right)\times\left(e^{\frac{-d_1}{P_S a_1\lambda_{SA}}}Ei\left(\frac{-d_1}{P_S a_1\lambda_{SA}}\right)-e^{\frac{-1}{P_S a_1\lambda_{SA}}}Ei\left(\frac{-1}{P_S a_1\lambda_{SA}}\right)\right), \quad (28)$$

where $c_1 = P_S a_1\lambda_{SA}/(P_R k\lambda_{RA})$, $d_1 = P_S a_1\lambda_{SA}/(P_T\lambda_{PA})$ and $Ei(\cdot)$ denotes the exponential integral function [39, Eq. (8.211)].

Proof: See Appendix D.

2) THE EC OF x_B

Setting $\mathcal{X} = \min\left(\gamma_{x_B}^R, \gamma_{x_B}^B\right)$, then, the CDF of $\mathcal{X}$, $F_{\mathcal{X}}(x)$, is defined as

$$F_{\mathcal{X}}(x) = \Pr\left(\min\left(\gamma_{x_B}^R, \gamma_{x_B}^B\right) < x\right) \quad (29)$$

From (29), the EC of x_B at B can be computed as

$$C_{x_B} = \frac{1}{\ln 2}\int_0^\infty \frac{1-F_{\mathcal{X}}(x)}{1+x}dx. \quad (30)$$

Theorem 4: The exact analytical expression of the EC of x_B at B in the considered NOMA-FD-CR system with the interference from PT is given by

$$C_{x_B} = \frac{n_2 k_2}{\ln 2}e^{m_2-\frac{u}{P_R\lambda_{RB}}}\times\left(\mathcal{A}\Theta(u,p_2,t)+\mathcal{B}\Theta(u,s_2,t)+\mathcal{C}\Theta(u,q_2,t)\right), \quad (31)$$

where $\mathcal{A} = \frac{-p_2}{(s_2-p_2)(q_2-p_2)}$, $\mathcal{B} = \frac{-s_2}{(p_2-s_2)(q_2-s_2)}$, $\mathcal{C} = \frac{-q_2}{(p_2-q_2)(s_2-q_2)}$, $m_2 = \frac{I_R+1}{P_S a_1\lambda_{SR}}$, $\Theta(u,m,t)$ is determined by (32), as shown at the bottom of the page, and $u = a_2/a_1$.

Proof: See Appendix E, F.

From (28) and (31), we can see that the ECs of x_A and x_B are independent of the target rates R_A and R_B. Instead, they depend on the power allocation coefficients a_1 and a_2 for A and B. On the other hand, P_T and P_R influence both C_{x_A} and C_{x_B}, i.e., larger P_T and P_R lead to smaller C_{x_A} and C_{x_B}. In contrast, the RSI I_R only impacts C_{x_B}.

V. NUMERICAL RESULTS

In this section, we provide analysis results together with Monte-Carlo simulation results to verify the derived mathematical expressions. We perform 10×2^{14} independent trials for each simulation. All nodes are located on a 1×1 area and are stationary in each communication period. Specifically, their locations are S(0;0), R(1;0), A(0.8;−1), B(2;0), PT(0;5) and PR(1;2). Let d_{XY} be the physical distance between two nodes X and Y. For free-space path loss transmission, we have the average channel gains $\lambda_{XY} = {d_{XY}}^{-\beta}$, where β, $2 \le \beta \le 6$, is the path loss exponent. Unless otherwise specified, the parameters setting are as follows: $P_T = 25$ dB, $\beta = 3$, $\gamma_1 = 0.5$, $\gamma_2 = 0.5$, $\phi = 0.1$, $\alpha = 0.6$, $N_0 = 1$, and $k = 0.03$. For the considered power-domain FD-NOMA-CR system, the power allocation coefficients are set as $a_1 = 0.2$ and $a_2 = 0.8$ for x_A and x_B, respectively.

Figs. 3 and 4 present the OPs and ECs of users A and B with MAIP and AIP constraints at R, i.e, the transmission power of R follows (11) and (8), respectively. We can see that the OPs of A and B corresponding to both MAIP and AIP constraints greatly reduce as I_P increases. Furthermore, the gap between them is larger with I_P. On the other hand, for the MAIP constraint, the OP of B is remarkably lower, while the OP of A is slightly higher compared with the AIP constraint, especially in the high SNR regime ($I_P > 15$ dB). It is because the transmission power of R in the case of MAIP constraint is higher than that in the case of AIP constraint. Therefore, the SINR at B increases, making the OP at B lower. Moreover, as the transmission power of R gets higher, the interference power at A caused by R increases, leading to an increase in the OP of A. However, this feature does not significantly affect the performance of the considered system because, in cognitive underlay systems, the transmission power of the secondary users is usually small because it is limited by the maximum tolerable interference threshold $\tilde{I}_P$. In other words, the fact that the OP of A increases slightly in the high SNR regime does not reduce the importance of (11) used to calculate the best transmission power of R. It is also important to remind that by using the average transmission power, the STs do not need to update the CSI of the interfering channel but still ensure the interference constraint at PRs. In Fig. 4, we see that in case that R applies the MAIP constraint, the EC of the signal C_{x_B} in low SNR regime ($I_P < 15$ dB) significantly improves while C_{x_A} is almost unchanged compared to the case that R applies the AIP constraint. In the high SNR regime ($I_P > 15$ dB), C_{x_A} corresponding to MAIP constraint becomes lower. However, this reduction does not affect the secondary users much because

$$\begin{aligned}\Theta(u,m,t) &= \int_0^u e^{-\frac{m_2 u}{t}+\frac{t}{P_R\lambda_{RB}}}\frac{dt}{t+m}\\ &= e^{\frac{m_2 u}{m}}Ei\left(-\frac{m_2 u}{m}(1+m/u)\right)-Ei(-m_2)-\frac{m}{P_R\lambda_{RB}}\left(e^{\frac{m_2 u}{m}}Ei\left(-\frac{m_2 u}{m}(1+m/u)\right)-Ei(-m_2)\right)\\ &+\frac{1}{P_R\lambda_{RB}}\left(ue^{-\frac{m_2}{2}}W_{-1,1/2}(m_2)\right)+\sum_{i=2}^{N}\frac{1}{i!}\left(\frac{1}{P_R\lambda_{RB}}\right)^i(-m)^i\left(e^{\frac{m_2 u}{m}}Ei\left(-\frac{m_2 u}{m}(1+m/u)\right)-Ei(-m_2)\right)\\ &+\sum_{i=2}^{N}\sum_{v=1}^{i}\sum_{j=0}^{v-1}\frac{1}{i!}\left(\frac{1}{P_R\lambda_{RB}}\right)^i(-1)^{i-v}m^{i-1-j}\binom{i}{v}\binom{v-1}{j}(m_2 u)^{\frac{j}{2}}u^{1+\frac{j}{2}}e^{-\frac{m_2}{2}}W_{-1-\frac{j}{2},\frac{j+1}{2}}(m_2). \quad (32)\end{aligned}$$

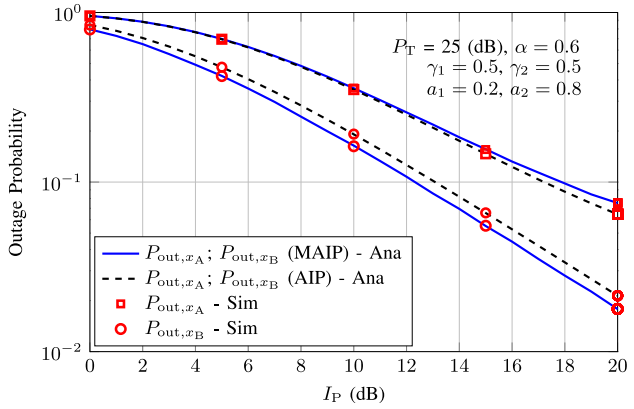

FIGURE 3. Outage probabilities of A and B versus $I_{\rm P}$ with MAIP and AIP constraints at R.

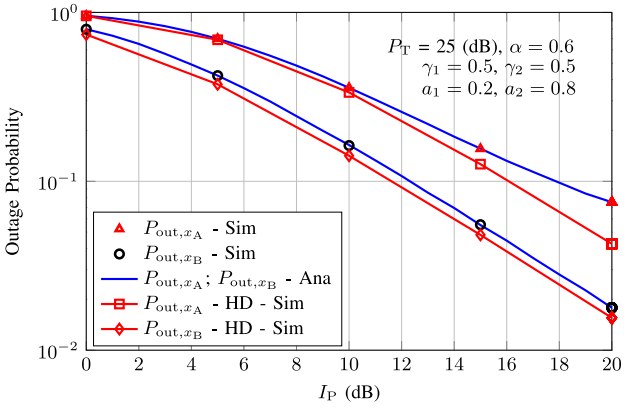

FIGURE 5. Outage probabilities of A and B versus the $I_{\rm P}$ for FD and HD transmission modes of R.

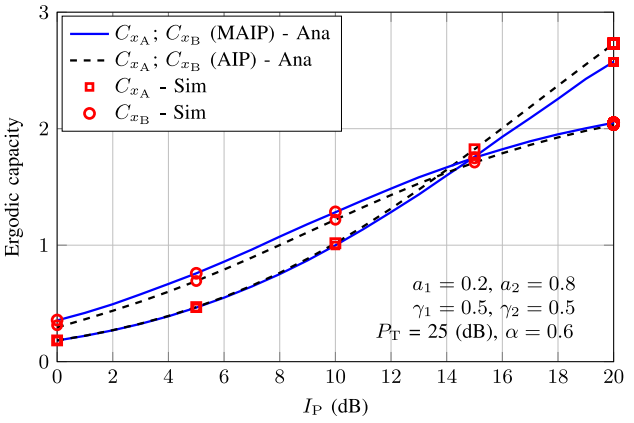

FIGURE 4. Ergodic capacities of A and B versus $I_{\rm P}$ with MAIP and AIP constraints at R.

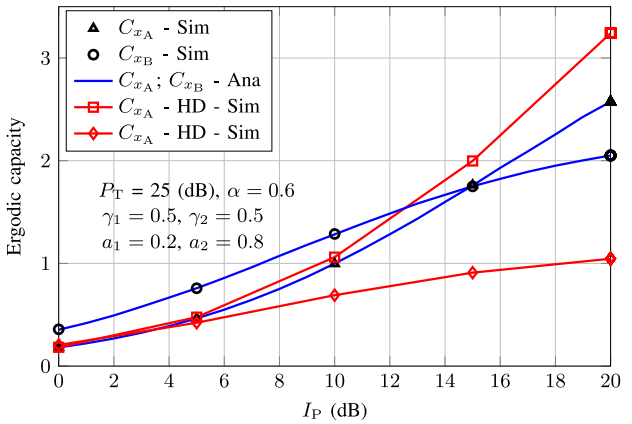

FIGURE 6. Ergodic capacities of $x_{\rm A}$ and $x_{\rm B}$ versus $I_{\rm P}$ for FD and HD transmission modes at R.

underlay cognitive systems usually operate in the low SNR regime.

Fig. 5 shows the OPs of two users A and B when interference threshold $I_{\rm P}$ changes from 0 dB to 20 dB for FD and HD transmission modes. As observed from Fig. 5, when R operates in FD mode, the OPs of both users A and B are higher than those when R operates in HD mode. It is because when R operates in FD mode, the interference from R to user A reduces the SINR of the received signal at A; thus, the outage performance of A is poorer. Meanwhile, the outage performance at B degrades due to the loop interference at R. However, the outage performances of A and B just reduce slightly in exchange for double spectrum efficiency. Specifically, as shown in Fig. 6, when R operates in FD mode, $C_{x_{\rm A}}$ decreases slightly, but $C_{x_{\rm B}}$ increases almost double compared to the case that R operates in HD mode. This feature indicates the advantage of the considered system with FD relay. We should remind that the purpose of using the relay R is to improve the signal quality of far user B. Therefore, although near user A suffers from a little EC reduction, better signal quality is achieved at B when R operates in FD mode. Furthermore, the considered system's spectral efficiency is doubled, and of course, the transmission delay from source S to far user B is reduced by a half.

Unlike most studies on the underlay cognitive environment, we consider the interference from the PT to the secondary system's performance. To see the effect of the interference from PT on the OPs of two destinations A and B, we depict in Fig. 7 the OPs of A and B as the functions of the transmission power of PT, $P_{\rm T}$. It is shown in Fig. 7 that the OPs of A and B rapidly increase when $P_{\rm T}$ gets higher. The communications of two destinations A and B are always in an outage when $P_{\rm T}$ exceeds a specific value. Besides, as expected, a larger allowed maximum interference threshold $I_{\rm p}$ results in smaller OPs of A and B.

Fig. 8 shows the impact of the transmission power $P_{\rm T}$ of PT on the ECs of $x_{\rm A}$ and $x_{\rm B}$ for different $I_{\rm P}$. We can see that as $P_{\rm T}$ is larger, the ECs of $x_{\rm A}$ and $x_{\rm B}$ are smaller. It is noted that $C_{x_{\rm A}}$ decreases faster than $C_{x_{\rm B}}$ because A is closer to the PT; thus, the interference from the PT to A is greater than that to B. From Figs. 7 and 8, we can see that the transmission power of PT, $P_{\rm T}$, greatly affects the OP and EC of both far and near users. Therefore, assuming the interference from the PT to the SRs is negligible as in [25], [29] may not reasonable.

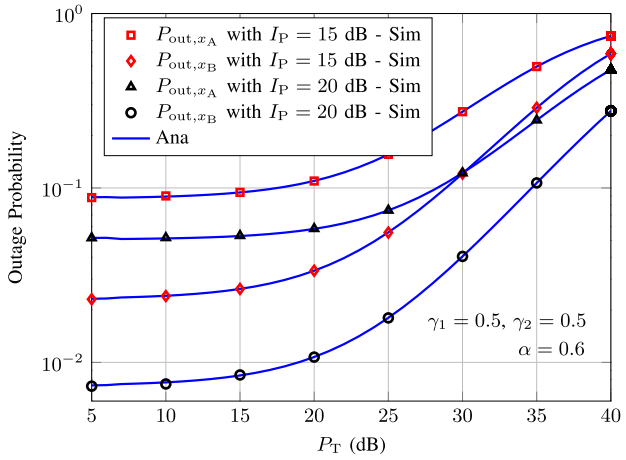

FIGURE 7. Outage probabilities of A and B versus P_T for different I_P.

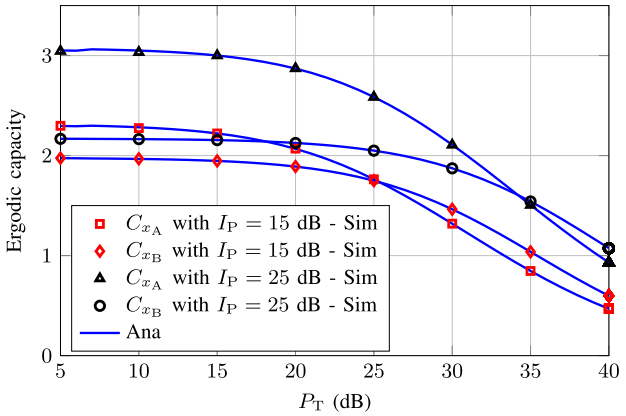

FIGURE 8. Ergodic capacities of x_A and x_B versus P_T for different I_P.

Based on the results in Figs. 7 and 8, we can observe that when $P_\text{T} > 20$ dB, both the OP and EC of the receiver in the secondary system drop very quickly, indicating the significant influence of the interference from the PT.

Fig. 9 presents the effect of the interference distribution coefficient α on the OPs of two users A and B for $P_\text{T} = 20$ dB, $I_\text{p} = 15$ dB. Since the transmission power of R increases linearly with α, the SINR of x_A also increases with α, making P_{out,x_A} continuously decrease. In contrast, P_{out,x_B} only decreases up to a certain value of α then sharply increases with α. It is because when increasing α to a certain value, the transmission power of R and the SINR at B quickly decreases, making P_{out,x_B} increase. From the results in 9, we can find $\alpha \approx 0.61$ at which P_{out,x_B} reaches the minimum value.

Fig. 10 depicts the influence of the interference distribution coefficient α on the ECs of x_A and x_B. It is noticed that, when α gets higher, the transmission power of S increases, leading to an increase in C_{x_A} and C_{x_B}. However, C_{x_B} increases up to a certain value of α, then quickly decreases when α approaches 1. It is because as α increases, the transmission power of S increases and the transmission power of R decreases, resulting in the reduced SINRs of the signal x_B in

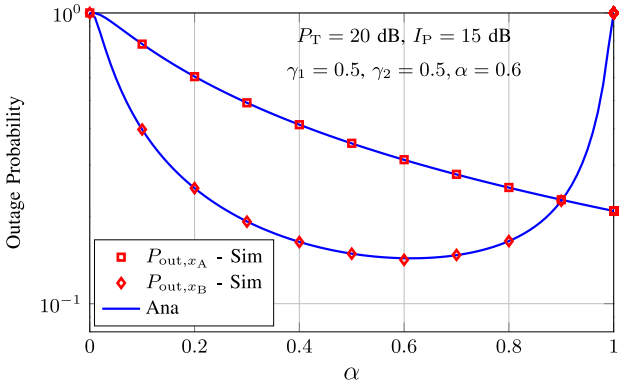

FIGURE 9. Effect of α on the outage probabilities of A and B.

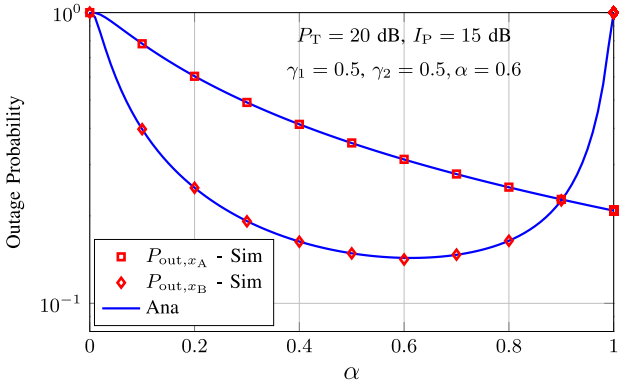

FIGURE 10. Effect of α on the ergodic capacities of x_A and x_B.

S $\rightarrow$ R and R $\rightarrow$ B stages. Due to C_{x_B} is determined by the capacity of the smaller hop, it cannot always increase with α. Based on the results in Fig. 10, we can find $\alpha \approx 0.67$ at which C_{x_B} reaches the maximum value.

VI. CONCLUSION

In this paper, we have analyzed a NOMA-CR relay system where an FD relay assists the communications from a base station to two users in the secondary network. We proposed the MAIP constraint for the relay to achieve maximum transmission power when operating in FD mode but still satisfied the interference constraint. Furthermore, we derived the exact closed-form expressions of the outage probabilities and the ergodic capacities of two users, taking into account the interference from PT to the secondary system. The Monte-Carlo simulations validate the derived mathematical expressions. Numerical results show that applying the MAIP constraint at the relay provides a significant improvement in the outage performance and ergodic capacity of the far user but only decreases the signal performance of near users slightly, especially in the low SNR regime. Furthermore, based on the MAIP constraint, we can adjust the average transmission power of S and R to satisfy the interference constraint at PR while do not need the instantaneous CSI of S–PR and R–PR interference channels.

APPENDIX A: SOLVE THE EQUATION 10

This appendix provides detailed solves to the following equation with respect to P_{R}.

$$\frac{P_{\mathrm{S}}\lambda_{\mathrm{SP}}}{P_{\mathrm{S}}\lambda_{\mathrm{SP}}-P_{\mathrm{R}}\lambda_{\mathrm{RP}}}e^{\frac{-I_{\mathrm{P}}}{P_{\mathrm{S}}\lambda_{\mathrm{SP}}}}-\frac{P_{\mathrm{R}}\lambda_{\mathrm{RP}}}{P_{\mathrm{S}}\lambda_{\mathrm{SP}}-P_{\mathrm{R}}\lambda_{\mathrm{RP}}}e^{\frac{-I_{\mathrm{P}}}{P_{\mathrm{R}}\lambda_{\mathrm{RP}}}}=\phi \tag{A.1}$$

For the sake of clarity, we set $\omega_1 = P_{\mathrm{S}}\lambda_{\mathrm{SP}}e^{-\frac{I_{\mathrm{P}}}{P_{\mathrm{S}}\lambda_{\mathrm{SP}}}}/\lambda_{\mathrm{RP}}$, $\omega_2 = P_{\mathrm{S}}\lambda_{\mathrm{SP}}/\lambda_{\mathrm{RP}}$, and $g = I_{\mathrm{P}}/\lambda_{\mathrm{RP}}$. Then, (A.1) can be represented as

$$\begin{aligned}&\frac{\omega_1}{\omega_2-P_{\mathrm{R}}}-\frac{P_{\mathrm{R}}}{\omega_2-P_{\mathrm{R}}}e^{-\frac{g}{P_{\mathrm{R}}}}=\phi\\&\Leftrightarrow \ln\left(\frac{\omega_1-\phi\omega_2}{P_{\mathrm{R}}}+\phi\right)=-\frac{g}{P_{\mathrm{R}}}.\end{aligned} \tag{A.2}$$

Setting $t = \frac{\omega_1-\phi\omega_2}{P_{\mathrm{R}}}+\phi$, $\omega_3 = \omega_1-\phi\omega_2$, we obtain

$$\ln(t) = -g\frac{t-\phi}{\omega_3} \Leftrightarrow \left(\frac{g}{\omega_3}t\right)e^{\frac{g}{\omega_3}t} = \frac{g}{\omega_3}e^{\frac{g\phi}{\omega_3}}. \tag{A.3}$$

Based on the definition of the Lambert function, we get the solution for (A.3) as

$$t = \frac{\omega_3}{g}\mathcal{W}\left(\frac{g}{\omega_3}e^{\frac{g\phi}{\omega_3}}\right) \tag{A.4}$$

where $\mathcal{W}(\cdot)$ denotes Lambert function [34].

Substituting ω_3 and g into (A.4) yields the solution of (A.1) as (11).

APPENDIX B: PROOF OF THEOREM 1

From (22), we have

$$P_{out,x_{\mathrm{A}}} = \begin{cases}1-\int_0^{\infty}\Pr\left(X>\frac{\gamma_2(w+1)}{P_{\mathrm{S}}(a_2-a_1\gamma_2)},X>\frac{\gamma_1(w+1)}{P_{\mathrm{S}}a_1}\right)\\ \quad\times f_W(w)\,dw & \text{if } a_2-a_1\gamma_2>0\\ 1 & \text{if } a_2-a_1\gamma_2\le 0\end{cases} \tag{B.1}$$

When $a_2-a_1\gamma_2 > 0$, we set $\theta = \max\left(\frac{\gamma_2}{(a_2-a_1\gamma_2)},\frac{\gamma_1}{a_1}\right)$, then we obtain

$$\begin{aligned}P_{\mathrm{out,A}} &= \int_0^{\infty}\Pr\left(X<\frac{\theta(w+1)}{P_{\mathrm{S}}}\right)f_W(w)\,dw\\&= \int_0^{\infty}\left(1-e^{-\frac{\theta(w+1)}{P_{\mathrm{S}}\lambda_x}}\right)f_W(w)\,dw.\end{aligned} \tag{B.2}$$

Applying (21), along with some mathematical manipulation, yields

$$\begin{aligned}P_{\mathrm{out,A}} = 1-e^{-\frac{\theta}{P_{\mathrm{S}}\lambda_{\mathrm{SA}}}}&\left(\frac{1}{P_{\mathrm{R}}k\lambda_{\mathrm{RA}}-P_{\mathrm{T}}\lambda_{\mathrm{PA}}}\right)\\&\times\int_0^{\infty}\left(e^{-w\left(\frac{\theta}{P_{\mathrm{S}}\lambda_{\mathrm{SA}}}+\frac{1}{P_{\mathrm{R}}k\lambda_{\mathrm{RA}}}\right)}-e^{-w\left(\frac{\theta}{P_{\mathrm{S}}\lambda_{\mathrm{SA}}}+\frac{1}{P_{\mathrm{T}}\lambda_{\mathrm{PA}}}\right)}\right)dw\end{aligned} \tag{B.3}$$

With the help of [39, Eq. (3.310)], we have the exact analytical expression of the OP of near user A as (23).

APPENDIX C: PROOF OF THEOREM 2

Firstly, we compute $\Pr\left(\gamma_{x_{\mathrm{B}}}^{\mathrm{R}}>\gamma_2\right)$ as

$$\begin{aligned}&\Pr\left(\gamma_{x_{\mathrm{B}}}^{\mathrm{R}}>\gamma_2\right)\\&=\Pr\left(\frac{P_{\mathrm{S}}a_2|h_{\mathrm{SR}}|^2}{P_{\mathrm{S}}a_1|h_{\mathrm{SR}}|^2+P_{\mathrm{T}}|h_{\mathrm{PR}}|^2+\mathrm{I_R}+1}>\gamma_2\right)\\&=\begin{cases}\int_0^{\infty}\Pr\left(|h_{\mathrm{SR}}|^2>\frac{\gamma_2(P_{\mathrm{T}}y+\mathrm{I_R}+1)}{P_{\mathrm{S}}(a_2-a_1\gamma_2)}\right)f_{|h_{\mathrm{PR}}|^2}(y)\,dy\\ \quad\text{if } a_2-a_1\gamma_2>0,\\ 0 \quad\text{if } a_2-a_1\gamma_2<0.\end{cases}\end{aligned} \tag{C.1}$$

When $a_2-a_1\gamma_2>0$, we have

$$\begin{aligned}&\Pr\left(\gamma_{x_{\mathrm{B}}}^{\mathrm{R}}>\gamma_2\right)\\&=\int_0^{\infty}e^{-\frac{\gamma_2(P_{\mathrm{T}}y+\mathrm{I_R}+1)}{P_{\mathrm{S}}(a_2-a_1\gamma_2)\lambda_{\mathrm{SR}}}}\frac{1}{\lambda_{\mathrm{PR}}}e^{-\frac{y}{\lambda_{\mathrm{PR}}}}dy\\&=\frac{1}{\lambda_{\mathrm{PR}}}e^{-\frac{\gamma_2(\mathrm{I_R}+1)}{P_{\mathrm{S}}(a_2-a_1\gamma_2)\lambda_{\mathrm{SR}}}}\int_0^{\infty}e^{-y\left(\frac{1}{\lambda_{\mathrm{PR}}}+\frac{\gamma_2P_{\mathrm{T}}}{P_{\mathrm{S}}(a_2-a_1\gamma_2)\lambda_{\mathrm{SR}}}\right)}dy\\&=e^{-\frac{\gamma_2(\mathrm{I_R}+1)}{P_{\mathrm{S}}(a_2-a_1\gamma_2)\lambda_{\mathrm{SR}}}}\frac{P_{\mathrm{S}}(a_2-a_1\gamma_2)\lambda_{\mathrm{SR}}}{P_{\mathrm{S}}(a_2-a_1\gamma_2)\lambda_{\mathrm{SR}}+P_{\mathrm{T}}\gamma_2\lambda_{\mathrm{PR}}}.\end{aligned} \tag{C.2}$$

Next, we compute $\Pr\left(\gamma_{x_{\mathrm{B}}}^{\mathrm{B}}>\gamma_2\right)$ as follows

$$\begin{aligned}&\Pr\left(\gamma_{x_{\mathrm{B}}}^{\mathrm{B}}>\gamma_2\right)\\&=\int_0^{\infty}\Pr\left(|h_{\mathrm{RB}}|^2>\frac{\gamma_2P_{\mathrm{T}}z+\gamma_2}{P_{\mathrm{R}}}\right)f_{|h_{\mathrm{PB}}|^2}(z)\\&=\frac{e^{-\frac{\gamma_2}{P_{\mathrm{R}}\lambda_{\mathrm{RB}}}}}{\lambda_{\mathrm{PB}}}\int_0^{\infty}e^{-z\left(\frac{\gamma_2P_{\mathrm{T}}}{P_{\mathrm{R}}\lambda_{\mathrm{RB}}}+\frac{1}{\lambda_{\mathrm{PB}}}\right)}dz=\frac{P_{\mathrm{R}}\lambda_{\mathrm{RB}}e^{-\frac{\gamma_2}{P_{\mathrm{R}}\lambda_{\mathrm{RB}}}}}{\gamma_2P_{\mathrm{T}}\lambda_{\mathrm{PB}}+P_{\mathrm{R}}\lambda_{\mathrm{RB}}}.\end{aligned} \tag{C.3}$$

Putting (C.1), (C.2), and (C.3) into (24), we get the exact closed-form expression of the OP of far user B as (25).

APPENDIX D: PROOF OF THEOREM 3

To find the expression of EC of x_{A}, we first derive the CDF of $\gamma_{x_{\mathrm{A}}}$, i.e.,

$$\begin{aligned}F_{\gamma_{x_{\mathrm{A}}}}(x) &= \Pr\left(\frac{P_{\mathrm{S}}a_1|h_{\mathrm{SA}}|^2}{P_{\mathrm{R}}|h_{\mathrm{RA}}|^2+P_{\mathrm{T}}|h_{\mathrm{PA}}|^2+1}<x\right)\\&=\int_0^{\infty}\Pr\left(|h_{\mathrm{SA}}|^2<\frac{x(w+1)}{P_{\mathrm{S}}a_1}\right)f_W(w)\,dw\\&=\int_0^{\infty}\left(1-e^{-\frac{x(w+1)}{P_{\mathrm{S}}a_1\lambda_{\mathrm{SA}}}}\right)f_W(w)\,dw,\end{aligned} \tag{D.1}$$

where $W = P_{\mathrm{R}}|h_{\mathrm{RA}}|^2+P_{\mathrm{T}}|h_{\mathrm{PA}}|^2$.

Applying (21), we obtain

$$\begin{aligned}&F_{\gamma_{x_{\mathrm{A}}}}(x)\\&=1-\int_0^{\infty}e^{-\frac{x(w+1)}{\xi_1}}\xi_2\left(e^{-\frac{w}{P_{\mathrm{R}}k\lambda_{\mathrm{RA}}}}-e^{-\frac{w}{P_{\mathrm{T}}\lambda_{\mathrm{PA}}}}\right)dw\end{aligned}$$

$$= 1 - e^{-\frac{x}{\xi_1}}\xi_2 \times \left(\int_0^\infty e^{-w\left(\frac{x}{\xi_1}+\frac{1}{P_R k \lambda_{RA}}\right)}dw - \int_0^\infty e^{-w\left(\frac{x}{\xi_1}+\frac{1}{P_T \lambda_{PA}}\right)}dw\right) \quad \text{(D.2)}$$

where $\xi_1 = P_S a_1 \lambda_{SA}$, and $\xi_2 = \frac{1}{P_R k \lambda_{RA} - P_T \lambda_{PA}}$.

Utilizing [39, Eq. (3.310)] yields

$$F_{\gamma_{x_A}}(x) = 1 - e^{-\frac{x}{\xi_1}}\xi_1\xi_2\left(\frac{1}{x+c_1} - \frac{1}{x+d_1}\right), \quad \text{(D.3)}$$

where $c_1 = P_S a_1 \lambda_{SA}/(P_R k \lambda_{RA})$, $d_1 = P_S a_1 \lambda_{SA}/(P_T \lambda_{PA})$.

Substituting (D.3) into (27), we obtain

$$C_{x_A} = \frac{\xi_1\xi_2}{(c_1-1)\ln 2}\int_0^\infty e^{-\frac{x}{\xi_1}}\left(\frac{1}{(x+1)} - \frac{1}{(x+c_1)}\right)dx - \frac{\xi_1\xi_2}{(d_1-1)\ln 2}\int_0^\infty e^{-\frac{x}{\xi_1}}\left(\frac{1}{(x+1)} - \frac{1}{(x+d_1)}\right)dx \quad \text{(D.4)}$$

Based on [39, Eq. (3.310)], we have the exact closed-form expression of the EC of x_A at A as (28).

APPENDIX E: COMPUTE $\Theta(u, m, t)$

We now compute $\Theta(u,m,t) = \int_0^u e^{-\frac{m_2 u}{t}+\frac{t}{P_R\lambda_{RB}}}\frac{dt}{t+m}$. Using Taylor series expansion, i.e.,

$$e^{\frac{t}{P_R\lambda_{RB}}} = \sum_{i=0}^N \frac{1}{i!}\left(\frac{t}{P_R\lambda_{RB}}\right)^i, \quad \text{(E.1)}$$

with N is the number of truncated terms in series expansion, $\Theta(u,m,t)$ can be expressed as

$$\Theta(u,m,t) = \sum_{i=0}^N \frac{1}{i!}\left(\frac{1}{P_R\lambda_{RB}}\right)^i \int_0^u e^{-\frac{m_2 u}{t}}\frac{t^i}{t+m}dt = \underbrace{\int_0^u e^{-\frac{m_2 u}{t}}\frac{1}{t+m}dt}_{I_a} + \underbrace{\frac{1}{P_R\lambda_{RB}}\int_0^u e^{-\frac{m_2 u}{t}}\frac{t}{t+m}dt}_{I_b} + \underbrace{\sum_{i=2}^N \frac{1}{i!}\left(\frac{1}{P_R\lambda_{RB}}\right)^i \int_0^u e^{-\frac{m_2 u}{t}}\frac{t^i}{t+m}dt}_{I_c}. \quad \text{(E.2)}$$

We first calculate I_a. By setting $t + m = tx$, or $t = m/(x-1)$, we have

$$I_a = e^{\frac{m_2 u}{m}}\left(\int_{1+m/u}^\infty \frac{e^{-\frac{m_2 u}{m}x}}{(x-1)}dx - \int_{1+m/u}^\infty \frac{e^{-\frac{m_2 u}{m}x}}{x}dx\right). \quad \text{(E.3)}$$

With the help of [39, Eq. (3.352.2)], yields

$$I_a = e^{\frac{m_2 u}{m}}Ei\left(-\frac{m_2 u}{m}(1+m/u)\right) - Ei(-m_2). \quad \text{(E.4)}$$

Next, we compute I_b as follows

$$I_b = \frac{1}{P_R\lambda_{RB}}\left(\int_0^u e^{-\frac{m_2 u}{t}}dt - m\int_0^u e^{-\frac{m_2 u}{t}}\frac{1}{t+m}dt\right). \quad \text{(E.5)}$$

It is noted that the second integral in parentheses of (E.5) is I_a, then, we have

$$I_b = \frac{1}{P_R\lambda_{RB}}\left(\int_0^u e^{-\frac{m_2 u}{t}}dt - mI_a\right) =^a \frac{1}{P_R\lambda_{RB}}\left(ue^{-\frac{m_2}{2}}W_{-1,1/2}(m_2) - mI_a\right), \quad \text{(E.6)}$$

where the equality $=^a$ is achieved by applying [39, Eq. (3.471.2)].

Plugging (E.4) into (E.6), we obtain

$$I_b = \frac{1}{P_R\lambda_{RB}}\left(ue^{-\frac{m_2}{2}}W_{-1,1/2}(m_2)\right) - \frac{m}{P_R\lambda_{RB}}\left(e^{\frac{m_2 u}{m}}Ei\left(-\frac{m_2 u}{m}(1+m/u)\right) - Ei(-m_2)\right). \quad \text{(E.7)}$$

Finally, we calculate I_c as follows

$$I_c = \sum_{i=2}^N \frac{1}{i!}\left(\frac{1}{P_R\lambda_{RB}}\right)^i (-m)^i \int_0^u e^{-\frac{m_2 u}{t}}\frac{1}{t+m}dt + \sum_{i=2}^N \sum_{v=1}^i \binom{i}{v}\frac{1}{i!}\frac{(-m)^v}{(P_R\lambda_{RB})^i}\int_0^u e^{-\frac{m_2 u}{t}}(t+m)^{v-1}dt. \quad \text{(E.8)}$$

Substituting (E.4) into the first integral in (E.8), we can rewrite I_c as

$$I_c = \sum_{i=2}^N \frac{1}{i!}\left(\frac{1}{P_R\lambda_{RB}}\right)^i (-m)^i I_{1a} + \sum_{i=2}^N \sum_{v=1}^i \sum_{j=0}^{v-1} \frac{1}{i!}\left(\frac{1}{P_R\lambda_{RB}}\right)^i (-1)^{i-v} m^{i-1-j} \times \binom{i}{v}\binom{v-1}{j}\int_0^u e^{-\frac{m_2 u}{t}}t^j dt. \quad \text{(E.9)}$$

Next, applying [39, Eq. (3.471.2)], we get

$$I_c = \sum_{i=2}^N \frac{1}{i!}\left(\frac{1}{P_R\lambda_{RB}}\right)^i (-m)^i \times \left(e^{\frac{m_2 u}{m}}Ei\left(-\frac{m_2 u}{m}(1+m/u)\right) - Ei(-m_2)\right) + \sum_{i=2}^N \sum_{v=1}^i \sum_{j=0}^{v-1} \frac{1}{i!}\left(\frac{1}{P_R\lambda_{RB}}\right)^i (-1)^{i-v} m^{i-1-j} \times \binom{i}{v}\binom{v-1}{j}(m_2 u)^{\frac{j}{2}} u^{1+\frac{j}{2}} e^{-\frac{m_2}{2}} W_{-1-\frac{j}{2},\frac{j+1}{2}}(m_2). \quad \text{(E.10)}$$

Finally, substituting (E.4), (E.7), and (E.10) into (E.1), we have the analytical expression of $\Theta(u,m,t)$ as (32).

APPENDIX F: PROOF OF THEOREM 4

Firstly, we find the CDF of $\mathcal{X} = \min\left(\gamma_{x_B}^R, \gamma_{x_B}^B\right)$. Based on the result in subsection IV-A2, from (24) and (25), we have the expression of CDF of $\mathcal{X}$ as follows

$$F_{\mathcal{X}}(x) = 1 - e^{-\frac{m_2 u}{u-x}+\frac{u-x}{P_R\lambda_{RB}}+m_2-\frac{u}{P_R\lambda_{RB}}} \times \frac{n_2(u-x)}{(u-x)+p_2}\frac{-k_2}{(u-x)+s_2}, \quad \text{(F.1)}$$

where $u = \frac{a_2}{a_1}$, $m_2 = \frac{\mathrm{I_R}+1}{P_S a_1 \lambda_{SR}}$, $n_2 = \frac{P_S a_1 \lambda_{SR}}{P_S a_1 \lambda_{SR} - P_T \lambda_{PR}}$, $p_2 = \frac{P_T \lambda_{PR} u}{P_S a_1 \lambda_{SR} - P_T \lambda_{PR}}$, $k_2 = \frac{P_R \lambda_{RB}}{P_T \lambda_{PB}}$, $s_2 = -\frac{P_R \lambda_{RB} + P_T \lambda_{PB} u}{P_T \lambda_{PB}}$.

It is noted that, the power allocation coefficients $a-1$ and a_2 satisfy the constraint $a_2 - a_1\gamma_2 > 0$, or $\gamma_2 < u$ with $u = a_2/a_1$, so that x_B can be decoded successfully. Therefore, the EC of x_B at B can be calculated as

$$C_{x_B} = \frac{1}{\ln 2}\int_0^u e^{-\frac{m_2 u}{u-x} + \frac{u-x}{P_R \lambda_{RB}} + m_2 - \frac{u}{P_R \lambda_{RB}}} \times \frac{n_2 (u-x)}{(u-x)+p_2} \frac{-k_2}{(u-x)+s_2} \frac{1}{x+1} dx. \quad \text{(F.2)}$$

Applying the change of variable $t = u - x$, we obtain

$$C_{x_B} = \frac{n_2 k_2 e^{m_2 - \frac{u}{P_R \lambda_{RB}}}}{\ln 2} \int_0^u \frac{t e^{-\frac{m_2 u}{t} + \frac{t}{P_R \lambda_{RB}}}}{(t+p_2)(t+s_2)(t+q_2)} dt, \quad \text{(F.3)}$$

where $q_2 = -(u+1)$.

Based on [39, Eq. (2.102)], we have

$$\frac{t}{(t+p_2)(t+s_2)(t+q_2)} = \frac{\mathcal{A}}{t+p_2} + \frac{\mathcal{B}}{t+s_2} + \frac{\mathcal{C}}{t+q_2}, \quad \text{(F.4)}$$

where $\mathcal{A} = \frac{-p_2}{(s_2-p_2)(q_2-p_2)}$, $\mathcal{B} = \frac{-s_2}{(p_2-s_2)(q_2-s_2)}$, $\mathcal{C} = \frac{-q_2}{(p_2-q_2)(s_2-q_2)}$.

Next, substituting (F.4) into (F.3), we get

$$\begin{aligned} C_{x_B} = {} & \frac{n_2 k_2}{\ln 2} e^{m_2 - \frac{u}{P_R \lambda_{RB}}} \mathcal{A} \int_0^u e^{-\frac{m_2 u}{t} + \frac{t}{P_R \lambda_{RB}}} \frac{t^{j-i}}{(t+p_2)} dt \\ & + \frac{n_2 k_2}{\ln 2} e^{m_2 - \frac{u}{P_R \lambda_{RB}}} \mathcal{B} \int_0^u e^{-\frac{m_2 u}{t} + \frac{t}{P_R \lambda_{RB}}} \frac{t^{j-i}}{(t+s_2)} dt \\ & + \frac{n_2 k_2}{\ln 2} e^{m_2 - \frac{u}{P_R \lambda_{RB}}} \mathcal{C} \int_0^u e^{-\frac{m_2 u}{t} + \frac{t}{P_R \lambda_{RB}}} \frac{t^{j-i}}{(t+q_2)} dt. \end{aligned} \quad \text{(F.5)}$$

Finally, applying the result of Appendix B, we get the exact analytical expression of the EC of x_B at B as (31).

REFERENCES

[1] S. Haykin, "Cognitive radio: Brain-empowered wireless communications," *IEEE J. Sel. Areas Commun.*, vol. 23, no. 2, pp. 201–220, Feb. 2005.

[2] T. Q. Duong, D. B. da Costa, M. Elkashlan, and V. N. Q. Bao, "Cognitive amplify-and-forward relay networks over Nakagami-*m* fading," *IEEE Trans. Veh. Technol.*, vol. 61, no. 5, pp. 2368–2374, Jun. 2012.

[3] A. Osseiran, F. Boccardi, V. Braun, K. Kusume, P. Marsch, M. Maternia, O. Queseth, M. Schellmann, H. Schotten, and H. Taoka, "Scenarios for 5G mobile and wireless communications: The vision of the METIS project," *IEEE Commun. Mag.*, vol. 52, no. 5, pp. 26–35, May 2014.

[4] F. Boccardi, R. W. Heath, Jr., A. Lozano, T. L. Marzetta, and P. Popovski, "Five disruptive technology directions for 5G," *IEEE Commun. Mag.*, vol. 52, no. 2, pp. 74–80, Feb. 2014.

[5] P. T. Hiep and T. M. Hoang, "Non-orthogonal multiple access and beamforming for relay network with RF energy harvesting," *ICT Exp.*, vol. 6, no. 1, pp. 11–15, Mar. 2020.

[6] A. W. Scott and R. Frobenius, *Multiple Access Techniques: FDMA, TDMA, and CDMA*. Hoboken, NJ, USA: Wiley, 2008, pp. 413–429.

[7] T. M. Hoang, B. C. Nguyen, L. T. Dung, and T. Kim, "Outage performance of multi-antenna mobile UAV-assisted NOMA relay systems over Nakagami-*m* fading channels," *IEEE Access*, vol. 8, pp. 215033–215043, 2020.

[8] M. T. P. Le, G. C. Ferrante, G. Caso, L. De Nardis, and M. Di Benedetto, "On information-theoretic limits of code-domain NOMA for 5G," *IET Commun.*, vol. 12, no. 15, pp. 1864–1871, Sep. 2018.

[9] Z. Zhang, Z. Ma, M. Xiao, Z. Ding, and P. Fan, "Full-duplex device-to-device-aided cooperative nonorthogonal multiple access," *IEEE Trans. Veh. Technol.*, vol. 66, no. 5, pp. 4467–4471, May 2016.

[10] T. M. Hoang, V. V. Son, N. C. Dinh, and P. T. Hiep, "Optimizing duration of energy harvesting for downlink NOMA full-duplex over Nakagami-*m* fading channel," *AEU-Int. J. Electron. Commun.*, vol. 95, pp. 199–206, Oct. 2018.

[11] T. M. Hoang, X. N. Tran, B. C. Nguyen, and L. T. Dung, "On the performance of MIMO full-duplex relaying system with SWIPT under outdated CSI," *IEEE Trans. Veh. Technol.*, vol. 69, no. 12, pp. 15580–15593, Dec. 2020.

[12] X. Lan, Y. Zhang, Q. Chen, and L. Cai, "Energy efficient buffer-aided transmission scheme in wireless powered cooperative NOMA relay network," *IEEE Trans. Commun.*, vol. 68, no. 3, pp. 1432–1447, Mar. 2020.

[13] T. M. Hoang, N. L. Van, B. C. Nguyen, and L. T. Dung, "On the performance of energy harvesting non-orthogonal multiple access relaying system with imperfect channel state information over Rayleigh fading channels," *Sensors*, vol. 19, no. 15, p. 3327, Jul. 2019.

[14] Z. Ding, Z. Zhao, M. Peng, and H. V. Poor, "On the spectral efficiency and security enhancements of NOMA assisted multicast-unicast streaming," *IEEE Trans. Commun.*, vol. 65, no. 7, pp. 3151–3163, Jul. 2017.

[15] X. Sun, S. Yan, N. Yang, Z. Ding, C. Shen, and Z. Zhong, "Short-packet downlink transmission with non-orthogonal multiple access," *IEEE Trans. Wireless Commun.*, vol. 17, no. 7, pp. 4550–4564, Jul. 2018.

[16] L. Lv, J. Chen, and Q. Ni, "Cooperative non-orthogonal multiple access in cognitive radio," *IEEE Commun. Lett.*, vol. 20, no. 10, pp. 2059–2062, Oct. 2016.

[17] L. Lv, L. Yang, H. Jiang, T. H. Luan, and J. Chen, "When NOMA meets multiuser cognitive radio: Opportunistic cooperation and user scheduling," *IEEE Trans. Veh. Technol.*, vol. 67, no. 7, pp. 6679–6684, Jul. 2018.

[18] S. Lee, T. Q. Duong, D. B. da Costa, D. B. Ha, and S. Q. Nguyen, "Underlay cognitive radio networks with cooperative non-orthogonal multiple access," *IET Commun.*, vol. 12, no. 3, pp. 359–366, Feb. 2018.

[19] T. M. C. Chu and H.-J. Zepernick, "Non-orthogonal multiple access for DF cognitive cooperative radio networks," in *Proc. IEEE Int. Conf. Commun. Workshops (ICC Workshops)*, May 2018, pp. 1–6.

[20] S. Arzykulov, G. Nauryzbayev, T. A. Tsiftsis, and B. Maham, "Performance analysis of underlay cognitive radio nonorthogonal multiple access networks," *IEEE Trans. Veh. Technol.*, vol. 68, no. 9, pp. 9318–9322, Jul. 2019.

[21] L. Bariah, S. Muhaidat, and A. Al-Dweik, "Error performance of NOMA-based cognitive radio networks with partial relay selection and interference power constraints," *IEEE Trans. Commun.*, vol. 68, no. 2, pp. 765–777, Feb. 2020.

[22] G. Im and J. H. Lee, "Outage probability for cooperative NOMA systems with imperfect SIC in cognitive radio networks," *IEEE Commun. Lett.*, vol. 23, no. 4, pp. 692–695, Apr. 2019.

[23] V. Aswathi and A. V. Babu, "Ensuring equal outage performance for downlink secondary users in full/half duplex cognitive NOMA systems," *IET Commun.*, vol. 14, no. 1, pp. 63–75, Jan. 2020.

[24] M. Mohammadi, B. K. Chalise, A. Hakimi, H. A. Suraweera, and Z. Ding, "Joint beamforming design and power allocation for full-duplex NOMA cognitive relay systems," in *Proc. IEEE Global Commun. Conf. (GLOBECOM)*, Dec. 2017, pp. 1–6.

[25] M. Mohammadi, B. K. Chalise, A. Hakimi, Z. Mobini, H. A. Suraweera, and Z. Ding, "Beamforming design and power allocation for full-duplex non-orthogonal multiple access cognitive relaying," *IEEE Trans. Commun.*, vol. 66, no. 12, pp. 5952–5965, Dec. 2018.

[26] X. Wang, M. Jia, Q. Guo, I. W.-H. Ho, and F. C.-M. Lau, "Full-duplex relaying cognitive radio network with cooperative nonorthogonal multiple access," *IEEE Syst. J.*, vol. 13, no. 4, pp. 3897–3908, Dec. 2019.

[27] V. S. Babu, N. Deepan, and B. Rebekka, "Performance analysis of cooperative full duplex NOMA system in cognitive radio networks," in *Proc. Int. Conf. Wireless Commun. Signal Process. Netw. (WiSPNET)*, Aug. 2020, pp. 84–87.

[28] C. K. Singh and P. K. Upadhyay, "Overlay cognitive IoT-based full-duplex relaying NOMA systems with hardware imperfections," *IEEE Internet Things J.*, early access, Sep. 8, 2021, doi: 10.1109/JIOT.2021.3111124.

[29] S. Kashyap and N. B. Mehta, "Sep.-optimal transmit power policy for peak power and interference outage probability constrained underlay cognitive radios," *IEEE Trans. Wireless Commun.*, vol. 12, no. 12, pp. 6371–6381, Dec. 2013.

[30] R. Zhang, "On peak versus average interference power constraints for protecting primary users in cognitive radio networks," *IEEE Trans. Wireless Commun.*, vol. 8, no. 4, pp. 2112–2120, Apr. 2009.
[31] H. Van Toan, V. Q. Bao, and H. Nguyen-Le, "Cognitive two-way relay systems with multiple primary receivers: Exact and asymptotic outage formulation," *IET Commun.*, vol. 11, no. 16, pp. 2490–2497, Nov. 2017.
[32] X. Kang, R. Zhang, Y.-C. Liang, and H. K. Garg, "Optimal power allocation strategies for fading cognitive radio channels with primary user outage constraint," *IEEE J. Sel. Areas Commun.*, vol. 29, no. 2, pp. 374–383, Feb. 2011.
[33] E. E. B. Olivo, D. P. M. Osorio, H. Alves, J. C. S. S. Filho, and M. Latva-Aho, "Cognitive full-duplex decode-and-forward relaying networks with usable direct link and transmit-power constraints," *IEEE Access*, vol. 6, pp. 24983–24995, 2018.
[34] R. M. Corless, G. H. Gonnet, D. E. G. Hare, D. J. Jeffrey, and D. E. Knuth, "On the LambertW function," *Adv. Comput. Math.*, vol. 5, no. 1, pp. 329–359, Dec. 1996.
[35] T. Riihonen, S. Werner, and R. Wichman, "Mitigation of loopback self-interference in full-duplex MIMO relays," *IEEE Trans. Signal Process.*, vol. 59, no. 12, pp. 5983–5993, Dec. 2011.
[36] D. Bharadia, E. Mcmilin, and S. Katti, "Full duplex radios," in *Proc. ACM SIGCOMM Conf.*, Aug. 2013, pp. 375–386.
[37] D. P. M. Osorio, E. E. B. Olivo, H. Alves, J. C. S. S. Filho, and M. Latva-Aho, "Exploiting the direct link in full-duplex amplify-and-forward relaying networks," *IEEE Signal Process. Lett.*, vol. 22, no. 10, pp. 1766–1770, Oct. 2015.
[38] X. Li, C. Tepedelenlioğlu, and H. Şenol, "Channel estimation for residual self-interference in full-duplex amplify-and-forward two-way relays," *IEEE Trans. Wireless Commun.*, vol. 16, no. 8, pp. 4970–4983, Aug. 2017.
[39] D. Zwillinger, *Table of Integrals, Series and Products*, 8th ed. Cambridge, MA, USA: Academic, 2014.

HOANG VAN TOAN received the B.S. degree in communication command from Telecommunications University, Ministry of Defense, Nha Trang, Vietnam, in 2002, the B.Eng. degree in electrical engineering from Le Quy Don Technical University, Hanoi, Vietnam, in 2006, the M.Eng. degree in electronics engineering from the Posts and Telecommunications Institute of Technology, Ho Chi Minh City, Vietnam, in 2011, and the Ph.D. degree from Le Quy Don Technical University, in 2018. His research interests include cognitive radio, energy harvesting, NOMA, and signal processing for wireless cooperative communications.

QUYET-NGUYEN VAN received the B.E. degree in information technology from the University of Information Technology, Vietnam National University, Ho Chi Minh City, Vietnam, in 2009, and the M.S. degree in information technology from Lac Hong University, Bien Hoa, Dong Nai, in 2015. His major research interests include computer science, networking, cloud computing, the IoT, and image processing.

TRAN MANH HOANG received the B.S. degree in communication command from Telecommunications University, Ministry of Defense, Nha Trang, Vietnam, in 2002, the B.Eng. degree in electrical engineering from Le Quy Don Technical University, Hanoi, Vietnam, in 2006, the M.Eng. degree in electronics engineering from the Posts and Telecommunications Institute of Technology, Ho Chi Minh City, Vietnam, in 2013, and the Ph.D. degree from Le Quy Don Technical University, in 2018. His research interests include energy harvesting, NOMA, and signal processing for wireless cooperative communications.

VAN-DUC PHAN received the M.S. degree from the Department of Electric, Electrical and Telecommunication Engineering, Ho Chi Minh City University of Transport, Ho Chi Minh City, Vietnam, and the Ph.D. degree from the Department of Mechanical and Automation Engineering, Da-Yeh University, Taiwan, in 2016. His research interests include sliding mode control, non-linear systems or active magnetics bearing, energy harvesting enabled cooperative networks, improving the optical properties, lighting performance of white LEDs, energy efficiency LED driver integrated circuits, and novel radio access technologies.

BUI VU MINH graduated in electrical and electronic engineering from Nguyen Tat Thanh University, Ho Chi Minh City, Vietnam, in 2015. He received the master's degree in electrical engineering from the Ho Chi Minh City University of Technology and Education, Ho Chi Minh City, in 2019. In 2014, he joined the Faculty of Mechanical, Electrical, Electronic and Automotive Engineering, Nguyen Tat Thanh University, and the Laboratory Practice Management, where he was a Lecturer, in 2017. His major research interests are wireless networks, robot, artificial neural networks, and power electronics.

PHAM THANH HIEP (Member, IEEE) received the B.E. degree in communications engineering from the National Defense Academy, Japan, in 2005; and the M.E. and Ph.D. degrees in physics, electrical and computer engineering from Yokohama National University, Yokohama, Japan, in 2009 and 2012, respectively. He was working as an Associate Researcher at Yokohama National University, from 2012 to 2015. He is currently a Lecturer at Le Quy Don Technical University, Hanoi, Vietnam. His research interests include the area of wireless information and communications technologies.

LE THE DUNG (Member, IEEE) received the B.S. degree in electronics and telecommunication engineering from the Ho Chi Minh City University of Technology, Ho Chi Minh City, Vietnam, in 2008, and the M.S. and Ph.D. degrees in electronics and computer engineering from Hongik University, Seoul, South Korea, in 2012 and 2016, respectively. From 2007 to 2010, he joined Signet Design Solutions Vietnam as a Hardware Design Engineer. He has been with Chungbuk National University as a Postdoctoral Research Fellow, since May 2016, and with Ton Duc Thang University as a Part-time Researcher, since November 2018. He has more than 60 papers in referred international journals and conferences. His major research interests include routing protocols, network coding, and network stability analysis and optimization in mobile *ad-hoc* networks, cognitive radio *ad-hoc* networks, and visible light communication networks. He was a recipient of the IEEE IS3C2016 Best Paper Award.